Test method

Analisys of the fatigue properties of different specimens of a 10% by weight short glass fibre reinforced polyamide 6.6

A. Bernasconi [a], F. Cosmi [b, *], D. Taylor [c]

[a] Politecnico di Milano, Dipartimento di Meccanica, Via La Masa 34, 20156, Milan, Italy
[b] Università degli Studi di Trieste, Dipartimento di Ingegneria ed Architettura, Via Valerio 6/4, 34127, Trieste, Italy
[c] Trinity College Dublin, Department of Mechanical and Manufacturing Engineering, College Green, Dublin 2, Ireland

Article history:
Received 1 July 2014
Accepted 27 August 2014
Available online 6 September 2014

1. Introduction

Nowadays, public opinion is increasingly oriented towards recycling of materials, due to waste proliferation, growth of material costs and reduction in the availability of resources. Short glass fibre reinforced plastics are promising substitutes for metallic materials in automotive applications. In a green technology framework, these materials can be obtained from the recycling of different industrial products, including several parts from the automotive sector itself, and will also lead to weight reductions that translate into lower fuel consumption and reduced operating costs.

In this context, it becomes crucial to understand the mechanical behavior of these materials, particularly when subjected to cyclic loads. In short fibre reinforced thermoplastic polymers, the static and fatigue stiffness and strength properties depend on the distribution of fibre lengths and orientations, which are determined by the molding process parameters [1–6]. The principal factors influencing the mechanical properties are, besides reinforcing material and matrix type, the fibre fraction, the sample geometry, the fibre length and fibre orientation distributions, and the environmental conditions, such as the test temperature and the frequency of the cyclic loads [7].

In this work, the effect of the sample geometry was investigated by comparing the mechanical, static and fatigue, properties of PA6.6GF10 specimens prepared according to two different standards: ISO 527-1a and ASTM D1822.

Among the other effects, a quantitative evaluation of the fibre microstructure and of its effects on defect propagation is a fundamental step for improving the design techniques for these materials, with particular reference to the application of fatigue loads that are typical of the automotive industry [8–11]. In recent years, micro-CT has proved to be a very effective and reliable method for assessing fibre structure in SFRP [12–19]. More recently, efforts have been made to apply the technique to study the damage

* Corresponding author. Francesca Cosmi Università degli Studi di Trieste, Dipartimento di Ingegneria ed Architettura, Via Valerio 6/4, 34127, Trieste, Italy. Tel.: +39 0405583431; fax: +39 0405583812.

E-mail addresses: andrea.bernasconi@polimi.it (A. Bernasconi), cosmi@units.it (F. Cosmi), DTAYLOR@tcd.ie (D. Taylor).

accumulation processes in these materials [20]. Among other issues, the micro-CT set-up requires samples of narrow gauge section allowing damage to be concentrated [20]. Since it might be difficult to identify *a priori* the damaged area in samples of constant section such as those of ISO 527-1a, the second geometry examined, ASTM D1822, exhibits a constant curvature, which allows one to concentrate the damage in the narrow area. A collection of data during interrupted fatigue tests on the ASTM D1822 samples, for later use in damage accumulation investigations, was the second aim of this experimental characterization. However, in order to relate the fatigue behavior observed in these smaller specimens with that derived from tests on larger standard specimens, a comparative investigation was conducted and the results are presented in this paper.

It is well known that the fatigue phenomenon is influenced by the viscous nature of polymeric materials: a polymeric material subjected to a sinusoidal cyclic load usually exhibits viscoelastic or viscoplastic behavior, characterized by a phase shift between the applied stress and the measured strain. The magnitude of this phase shift depends on how much the material behavior is elastic rather than viscous: in the limit case of a perfectly elastic material, there is no phase shift, while for the ideal case of a perfectly viscous material the phase shift is equal to a quarter of the period. Hysteresis loops are observed and energy dissipation takes place through thermal dissipation. The onset of important thermal phenomena can shift the failure cause from mechanical fatigue to thermal fatigue. Conversely, if the hysteresis loop is sufficiently small or the material properties allow efficient dissipation of the produced heat, failure will still be governed by mechanical fatigue [21–23]. Typically, for short glass fiber reinforced polyamides in the conditioned state, the number of cycles to failure is dependent on test frequency, as found in [24] for a PA6GF30. The dependence on test frequency can be interpreted in terms of self-heating effects, and temperature effects are strictly related to the specimen geometry. In order to investigate the thermal behavior, a fatigue thermal analysis was performed on the ISO samples. This type of analysis was not possible on the AMST specimens, due to their small dimensions.

2. Specimens

The specimens used in this study were made of SGFR polyamide 6.6 with 10% fibre content by weight (PA6.6GF10), conditioned at 23°C and 50% relative humidity. As already mentioned, two sample geometries were tested: the ASTM D1822 (9.6 mm^2 section, constant curvature) and the ISO 527-1a (40 mm^2, constant section). A total number of 30 ASTM D1822 samples, depicted in Fig. 1, and 25 ISO 527 samples, Fig. 2, were used.

All specimens were obtained by injection moulding. The polymer melt behaves like a viscous fluid and the final mechanical properties obtained in the injection moulding process are not only a consequence of the reinforcement content but also of the fibre orientation, which is determined by the process dynamics and the mould cavity geometry, as already mentioned in the Introduction.

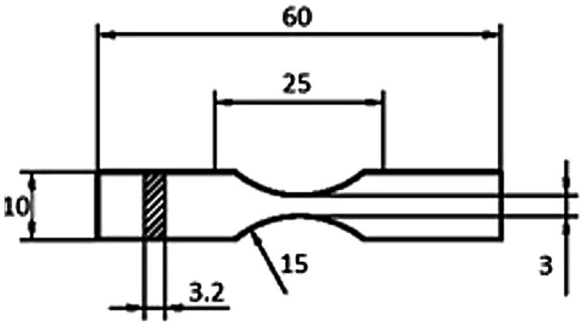

Fig. 1. The ASTM D1822 geometry.

3. Experimental procedures

A servo-hydraulic Instron 8801-A2 machine with a 100kN load cell was employed for tensile and fatigue tests. Strains were recorded for the ISO 527 samples by means of an extensometer with 50mm base length. For the ASTM D1822 specimens, the movements of the mobile grip were directly recorded.

3.1. Tensile tests

Four tensile tests for each specimen geometry were performed with a crosshead speed of 1mm/s at ambient conditions of 20°C, 60% humidity.

3.2. Fatigue tests

Fatigue tests at different stress levels were run for each type of geometry by applying sinusoidal tensile loads of constant amplitude in load control mode. The ambient conditions of 19 °C temperature and 60% humidity may have undergone slight fluctuations around these values. Tests consisted of tension to tension load cycles at 2Hz, with a minimum to maximum load ratio $R = 0.1$ for all tests. Failure was defined by specimen separation.

Fatigue tests conducted at different stress levels allowed for identification of the stress level corresponding to a fatigue life of 10^5 cycles. Further fatigue tests were performed at this stress level on the ASTM samples and interrupted at different stages of the corresponding average fatigue life, 20%, 40%, 60%, 70%, 80%, 90% respectively. During the interrupted fatigue tests on the ASTM D1822 samples, the maximum and minimum strain values over each cycle were collected. The complete stress-strain cycle was also gathered every 1000 cycles.

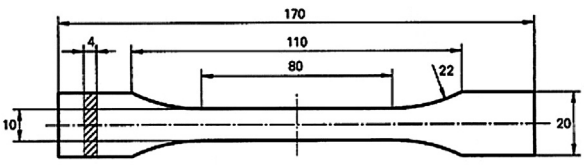

Fig. 2. The ISO 527-1A geometry.

Table 1
Fatigue tests parameters for the thermal analyses.

Specimen	1	2	3	4
σ_{max} (MPa)	31	49	48	47
R	0.1	0.1	0.1	0.1
N	9235	44100	78524	> 370000

3.3. Thermal analysis

For the thermal analysis, the surface temperatures along the longitudinal centerline of four ISO 527 samples were acquired under fatigue loading in the range between 10,000 and 200,000 cycles using an infrared camera (thermaCAM P25). Before testing, the specimens were painted with a matt black paint of emissivity 0.95 to improve the camera accuracy and to bring the specimens into the sharpest focus possible with the available camera lens. The thermal tests were conducted on fresh test pieces but of the same geometry as those used to derive the fatigue stress-life curve. The new specimens were tested at different load levels, summarized in Table 1, exploring the life range between 10,000 and 250,000 life cycles.

Temperatures were recorded every 3 minutes for the first 45 minutes and thereafter every 30 minutes. During these tests, the complete stress-strain cycle was also gathered every 1,000 cycles.

4. Results and discussion

4.1. Tensile tests

The stress-strain curves for the two types of specimen are depicted for comparison in Fig. 3. Despite being obtained from the same polyamide 6.6 reinforced by 10% w short glass fibres, the two types of specimen exhibit very different behavior, as confirmed by the tensile test results (average value for each geometry) collected in Table 2. The Young's modulus of the dumbbell ISO 527 specimens was 36% higher than that of the hourglass ASTM D1822 specimens. However, the value of the Young's modulus of the ASTM D1822 specimens was evaluated based on the displacement of the grips and, therefore, cannot be compared with the more accurate measurements conducted on the ISO 527 specimens using an extensometer.

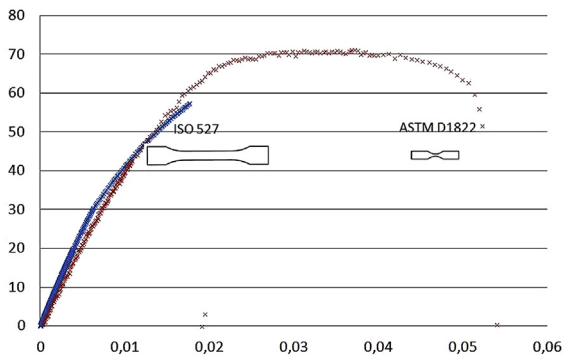

Fig. 3. Stress-strain curves for the ASTM D1822 and the ISO 527 specimens.

Table 2
Young's modulus *E*, Yield stress (0.2 % off-set), Ultimate tensile strength *UTS*, and percent elongation at break for the two geometries investigated.

	Young's modulus *E* (MPa)	Yield stress (0.2 % off-set) (MPa)	Ultimate tensile strength *UTS* (MPa)	Elongation at break (%)
ASTM D1822	(4481)	59	72	(5.4)
ISO 527	5119	42	56	3.0

Conversely, the yield stress at 0.2 % offset and the ultimate tensile strength of the ASTM D1822 specimens were respectively 29% and 22% higher than those of the ISO 527 samples. The increase in elongation at break, shown in Fig. 3, between the dumbbell and the hourglass specimens is particularly noteworthy, although similar considerations about the accuracy of the measurement of the strain at break for ASTM D1822 specimens apply as in the case of the Young's modulus values.

4.2. Fatigue tests

The results of the fatigue tests are reported in Fig. 4, which is a bi-logarithmic plot of the maximum applied stress versus the number of cycles to failure N_f. The test results are linearly interpolated to obtain the corresponding S–N curves (Wöhler curves), which are superimposed on the experimental results in the graph. Although very different properties can be observed for the two specimen types, the S-N curves appear to be nearly parallel to each other. Assuming a $\sigma_{max} = \sigma_f N^{\alpha}$ form for the S-N curves, the fatigue strength exponent α, slope of the S-N curve and the fatigue strength coefficient σ_f are shown in Table 3.

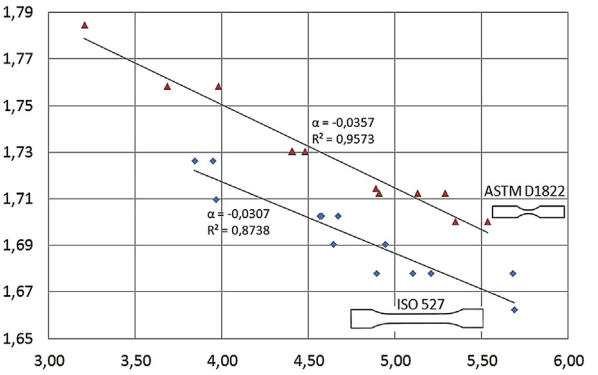

Fig. 4. S-N curves of conditioned PA6.6GF10 ISO 527 and ASTM D1822 samples tested at R = 0.1, 2Hz frequency and ambient temperature of 19°C, 60% humidity.

Table 3
Values of the fatigue strength coefficients and exponents of PA6.6GF10 for the two geometries investigated.

	Fatigue strength exponent α	Fatigue strength coefficient σ_f (MPa)
ASTM D1822	−0.0357	78
ISO 527	−0.0307	69

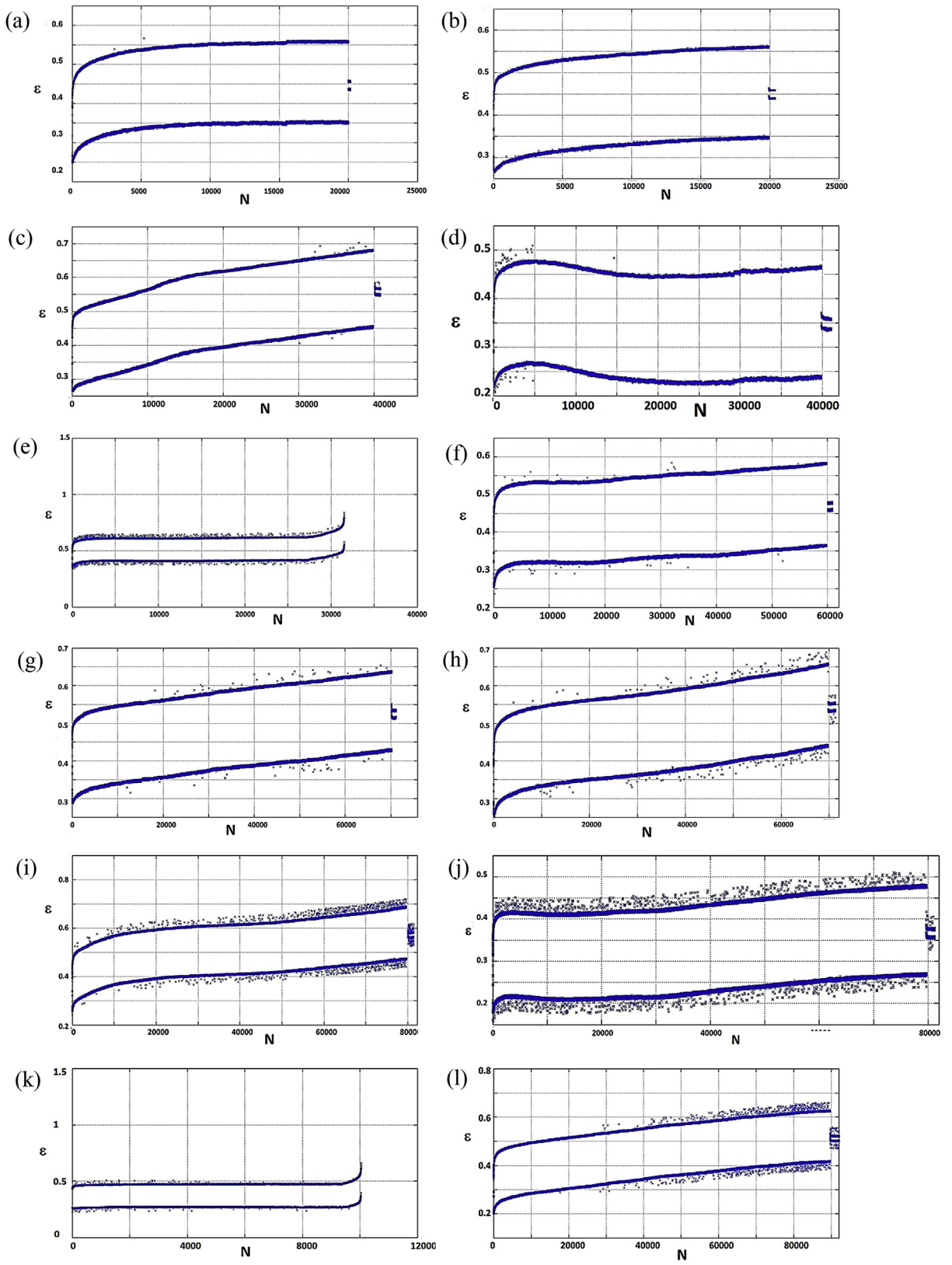

Fig. 5. The maximum and minimum strain values over each cycle of the samples tested at: 20% (a) and (b), 40% (c) and (d), 60% (e) (failed at 32521 cycles) and (f), 70% (g) and (h), 80% (i) and (j), 90% (k) (failed at 11003 cycles) and (l) of fatigue life respectively.

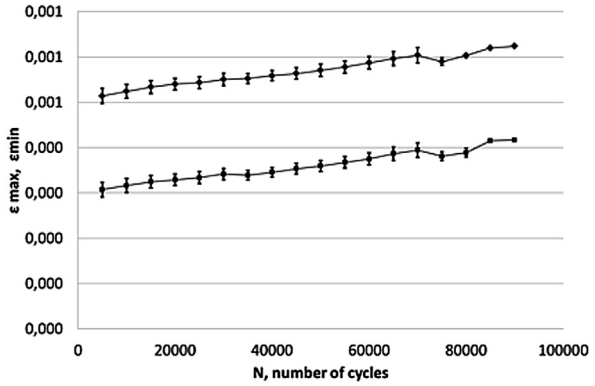

Fig. 6. The maximum and minimum strain values (average and error bar) recorded every 5,000 cycles in all the interrupted tests of the ASTM D1822 specimens.

The stress level corresponding to a life of 10^5 cycles was 52 MPa for the ASTM D1822 and 48 MPa for the ISO527 specimens. The differences in the fatigue behavior (the fatigue stress coefficient obtained using ASMT D1882 specimens is 15% higher than that obtained using the ISO 527 specimens) are almost in agreement with the observed tensile behavior (UTS of ASTM D1822 is 28.5% higher than that of the ISO 527 specimen). A possible explanation of these differences is the different fibre orientation pattern. A narrower gauge section and a width varying continuously with a constant curvature radius are likely to have induced a higher degree of alignment of the reinforcing fibres with the specimen axis. On the other hand, the ISO 527 specimen, having a thicker section and a long gauge section with constant width, is known to display the usual shell-core structure, with fibres aligned along the specimen's axis in the shell layers and a much more scattered fibre orientation distribution in the central part of the section.

Another possible source of the observed differences in the mechanical behavior could be the thermal behavior, related to the hysteresis of the material. Hysteresis implies energy dissipation through heat exchange, and in turn, the shape of the gauge section influences the heat exchange. Therefore, the cyclic behavior and the thermal behavior have also been investigated.

Two specimens were used for each stress level in the interrupted fatigue tests run on the ASTM D1822 specimens. The tests were interrupted at 20,000, 40,000, 60,000, 70,000, 80,000 and 90,000 cycles. One of the samples failed at 32,521 cycles and another at 11,003 cycles, before reaching the expected end of the tests, 60,000 and 90,000 cycles respectively. The maximum and minimum strain values recorded over each cycle are shown in Fig. 5.

Since the maximum and minimum strain recordings differ from one sample to another, a graph of the maximum and minimum strain values recorded every 5,000 cycles (average value and error bar) in all the interrupted tests appears to be more significant, and is shown in Fig. 6. It can, therefore, be observed that the maximum and the minimum strain values increase by the same amount, i.e. the difference between the maximum and the minimum strain is almost constant in the examined life range.

The hysteresis loops of the ASTM samples were also gathered every 1,000 cycles during the interrupted fatigue tests. The graph showing the last recorded hysteresis loops for each fatigue life level is shown in Fig. 7. The hysteresis loops appear even at fairly moderate stress levels, due to phase shifts between applied stresses and measured strains, which are never in a linear relationship. The progression of the hysteresis loops along the strain axis throughout the lives of the specimens is indicative of cyclic creep, while cyclic softening is not evident.

4.3. Thermal analysis

The surface temperature recorded at different stress levels for the ISO samples is reported in Fig. 8 as a function of the number of cycles. Labels inside the plot area indicate the applied maximum stress. The test conducted at 47.3 MPa was interrupted at 370,000 cycles, whereas the other three tests ended at specimen separation.

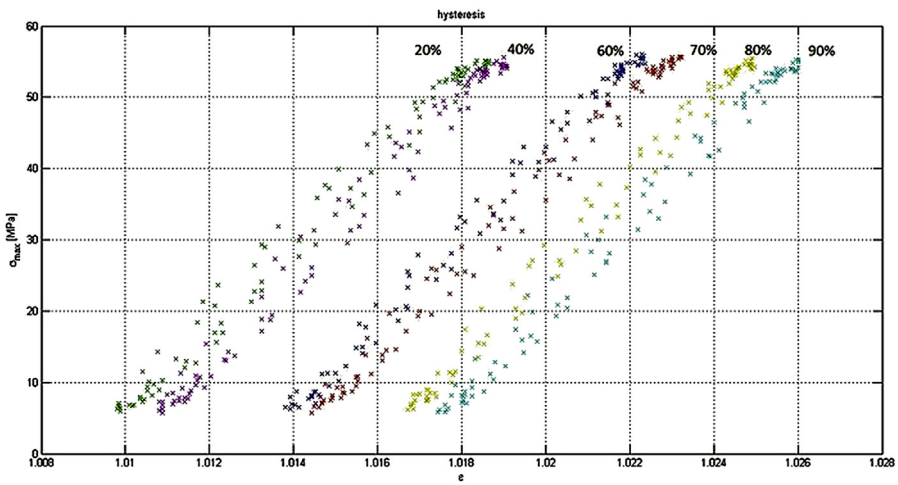

Fig. 7. Last recorded hysteresis loops for each fatigue life level in the interrupted tests of the ASTM D1822 specimens. Percent numbers indicate the specimen life stage at recording.

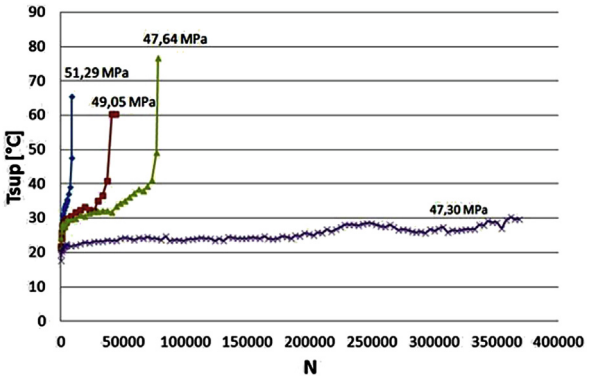

Fig. 8. Surface temperature for ISO samples.

It appears that surface temperature increases rapidly during the first stage of the tests, then the rate of temperature increase stays constant for most of the fatigue life, with a steep rise taking place during the very last cycles. The variation of the surface temperature with the number of cycles follows a sigmoidal curve similar to that of the maximum strain. Temperature fluctuations can be observed in the case of the specimen tested at the lowest stress level, presumably due to the fluctuations in the ambient temperature (it was not possible to conduct the test in a temperature controlled environment).

By analyzing the temperature data in the range corresponding to the secondary stage, it appears that the average temperature almost coincides with the temperature at half the fatigue life ($N_f/2$), as is reported in Table 4. This coincides with similar observations reported in [24] for a similar material, containing 30% by weight reinforcing fibres. Compared to the data reported in [24], average temperature values are similar for similar fatigue lives, although final peak values are much higher in the case of the less reinforced material presented in this work.

5. Conclusions

The ASTM and ISO samples exhibit very different static and dynamic properties. This result is mainly due to the differences in the mould geometry, which is one of the parameters influencing the polymer flow into the mould and, presumably, the reinforcing fibre distribution, which in turn determines the mechanical properties obtained in the specimen.

The trend of the maximum and minimum strains and the shifts in hysteresis loops along the strain axis in the interrupted fatigue tests of the ASTM samples are similar. With each 20% increase in life cycles, the area enclosed by the hysteresis loops grows by about 10%.

The thermal behavior of the ISO samples is characterized by a rapid rise in the surface temperature at the beginning and at the end of the tests. A lower increase (7°C for high stress tests and 3°C for low stress tests) was found in the remaining fatigue life, confirming the trend found in [24] for a PA6GF30. At present, the ASTM samples subjected to the interrupted fatigue tests are being further analyzed by means of micro-computed tomography, a technique which allows a complete 3D reconstruction of the internal structure of the sample, evidencing both fibre architecture and micro-void distribution. The purpose of this additional investigation is a better understanding of the damage nucleation and progression phenomena, a necessary step for the development of accurate predictive models of the fatigue behavior of SFRP materials.

Table 4
Values of T_{avg}, average temperature in the secondary phase, of Tat $N_f/2$, temperature at $N_f/2$ and percentage difference.

	T_{avg} (°C)	Tat $N_f/2$ (°C)	diff %
Sample 51.29 MPa	35.8	34.3	4.2
Sample 49.05 MPa	34.75	33.2	4.4
Sample 47.64 MPa	34.45	33.4	3.1

Conflict of interest statement

All authors certify that they have no affiliations with or involvement in any organization or entity with any financial interest, or non-financial interest in the subject matter discussed in this manuscript.

Acknowledgements

Specimens were kindly provided by Radici Plastics.

References

[1] J.J. Horst, Influence of Fibre Orientation on Fatigue of Short Glass-fibre Reinforced Polyamide, PhD Thesis, TU Delft, Netherland, 1997.
[2] J. Karger-Kocsis, K. Friedrich, Skin-core morphology and humidity effects on the fatigue crack propagation of PA-6.6, Plast. Rubber Compos. Process. Appl. 12 (1989) 63–68.
[3] S. Fu, B. Lauke, Effects of fiber length and fiber orientation distributions on the tensile strength of short-fiber-reinforced polymers, Compos. Sci. Technol. 56 (1996) 1179–1190.
[4] A. Bernasconi, F. Cosmi, Fibre Orientation at Notches and Fatigue Behaviour of Short Fibre Reinforced Polyamide, ICCM 17 Edinburgh, 2009.
[5] A. Bernasconi, F. Cosmi, Experimental Analysis of Fibre Orientation in Injection Moulded Plates Made of Short Fibre Reinforced Polyamide, ECCM-14 Budapest, 2010.
[6] A. Bernasconi, P. Davoli, C. Armanni, Fatigue strength of a clutch pedal made of reprocessed short glass fibre reinforced polyamide, Int. J. Fatigue 1 (2010) 100–107.
[7] N. Jia, V.A. Kagan, Effects of time and temperature on the tension-tension fatigue behavior of short fiber reinforced polyamides, Polym. Compos. 19 (4) (1998) 408–414.
[8] S. Piment, et al., Mechanical analysis and toughening mechanisms of a multiphase recycled CFRP, CSTE 70 (2010) 1713–1725.
[9] M. Schoßig, et al., ESEM investigations for assessment of damage kinetics of short glass fibre reinforced thermoplastics – results of in situ tensile tests coupled with acoustic emission analysis, CSTE 71 (2011) 257–265.
[10] J.H. Sul, B.G. Prusty, T. Ray, Prediction of low cycle fatigue life of short fibre composites at elevated temperatures using surrogate modelling, Compos. B Eng. 42 (6) (2011) 1453–1460.
[11] B. Klimkeit, et al., Multiaxial fatigue life assessment for reinforced polymers, Int. J. Fatigue 33 (6) (2011) 766–780.
[12] A. Bernasconi, F. Cosmi, D. Dreossi, Comp. Scie. Tech. 68 (2008) 2574–2781.
[13] F. Cosmi, A. Bernasconi, Elasticity of short fibre reinforced polyamide: morphological and numerical analysis of fibre orientation effects, Mater. Eng. 17 (2010) 6–10.
[14] A. Bernasconi, F. Cosmi, E. Zappa, Combined effect of notches and fibre orientation on fatigue behaviour of short fibre reinforced polyamide, Strain 46 (2010) 435–445.

[15] F. Cosmi, Local anisotropy and elastic properties in a short glass fibre reinforced polymer composite, Strain 47 (2011) 215–221.
[16] F. Cosmi, A micro-mechanical model of the elastic properties of a short fibre reinforced polyamide, Procedia Eng. 10 (2011) 2135–2140.
[17] A. Bernasconi, F. Cosmi, Analysis of the dependence of the tensile behaviour of a short fibre reinforced polyamide upon fibre volume fraction, length and orientation, Procedia Eng. 10 (2011) 2129–2134.
[18] F. Cosmi, A. Bernasconi, N. Sodini, Phase contrast micro-tomography and morphological analysis of a short carbon fibre reinforced polyamide, Comp. Scie. Tech. 71 (2011) 23–30.
[19] A. Bernasconi, F. Cosmi, P.J. Hine, Analysis of fibre orientation distribution in short fibre reinforced polymers: a comparison between optical and tomographic methods, Comp. Scie. Tech. 72 (2012) 2002–2008.
[20] F. Cosmi, A. Bernasconi, Micro-CT investigation on fatigue damage evolution in short fibre reinforced polymers, Compos. Sci. Technol. 79 (2013) 70–76.
[21] H. Nouri, F. Meraghni, P. Lory, Fatigue damage model for injection-molded short glass fibre reinforced thermoplastics, Int. J. Fatigue 31 (5) (2009) 934–942.
[22] B. Harris, Fatigue in Composites: Science and Technologies of the Fatigue Response of Fibre-reinforced Plastics, in: Woodhead Publishing Series in Composites Science and Engineering, 16, 2003.
[23] M.G. Rui, Creep and Fatigue in Polymer Matrix Composites, in: Woodhead Publishing Series in Composites Science and Engineering, 32, 2011.
[24] A. Bernasconi, M.R. Kulin, Effect of frequency upon fatigue strength of a short glass fiber reinforced polyamide 6: a superposition method based on cyclic creep parameters, Polym. Compos. 30 (2009) 154–161.